Tuijin Jishu/Journal of Propulsion Technology
ISSN: 1001-4055
Vol. 45 No. 1 (2024)

A Numerical Study on Performance of NACA 2418 Airfoil

Md. Zishan Ahmad[1], Arka Banerjee[2]*, Bishal Murmu[1], Sk Saidul[1]

[1] *UG Student, Department of Mechanical Engineering, Dr. B.C. Roy Engineering College, Durgapur, West Bengal, India*

[2] *Assistant Professor, Department of Mechanical Engineering, Dr. B.C. Roy Engineering College, Durgapur, West Bengal, India, ORCID ID: 0000-0001-9329-4033*

Abstract: The present research is on the 2-D flow simulation and performance optimization of an aerofoil using CFD software ANSYS-Fluent. The aerofoil model NACA-2418 is chosen for the investigation for its rising popularity in training aircrafts. Our motive is to investigate various fluid-dynamic aspects and to optimize its performance for economic use. Geometry of the aerofoil NACA-2418 is prepared and an asymmetric mesh is created in ANSYS-mesh. Optimum grid size is achieved by a suitable grid-independence study. The standard k-ε model has been used for turbulence modelling. Validation with the experimental results proved the CFD-model to fit accurately for the case. Variation of lift coefficient, drag coefficient and lift-to-drag ratio is explained with fluid dynamic visualization obtained from CFD results. An optimum Lift-to-drag ratio is found for the angle of attack lying near the range of 5º angle of attack for the present geometry.

Keywords*: CFD, NACA 2418, Angle of attack, Airfoil characteristics, lift-to-drag ratio*

1. Introduction

The NACA 2418 stands as proof of legacy of National Advisory Committee for Aeronautics (NACA), Describing the NACA's legacy, The 2418 Aerofoil has emerged as a leading figure in aerodynamic research, affecting wind turbines, aircraft, design, Unmanned aerial vehicles (UAVs), and educational programs. Its practical value is illustrated by its application in general aviation, where its optimum lift and haul characteristics support in the maintaining the stability of light aircraft. In addition, the versatile nature of the aerofoil also applies to unmanned aerial vehicles (UAVs), focusing its important role in current aviation technologies. When it deals with teaching, the NACA 2418 is a useful resource for teaching aerodynamics concepts to future aerospace engineers and hobbyists. The NACA 2418 aerofoil is widely utilized in the aviation and aerospace industries. The chosen aerofoil model NACA 2418 is one of the most suitable aerofoil model for research and investigation purposes, which has also resulted in its increasing popularity among researchers.

Graham et al. [1] selected the aerofoil models NACA 0018 and NACA 2418 based on initial investigations. They observed that these aerofoil models perform better with maximum width of 18% when placed within vertical axis wind turbines because, wider aerofoils performs better at inferior tip speeds. The lift and drag coefficients of the aerofoils were compared for estimating the most enhanced lift-drag ratio (L/D). Based upon the results, which were derived from the experiments and researches, it was found that the aerofoil NACA 0018 is more appropriate than the aerofoil model NACA 2418. Hence, it can be observed that, the capability of the aerofoil model NACA 2418 is better in free airflow as compared to wind turbines. The extended width if the aerofoil model provides it with better airflow over the body, that generates an enhanced lift-drag ratio in free air as compared to wind turbines. Abood and Abdulrazzaq [2] used COMSOL Multiphysics Simulation Program for calculating the lift and drag coefficient for various two-dimensional aerofoil models. Along with that, they also focused on finding the glide ratio of each of these aerofoil models, such as NACA 2412, NACA 2415,

NACA 2418, NACA 4412, and NACA 4415 during their study of these aerofoil models. They also experimented on the above aerofoil models by altering the angle of attack (α) ranging from 0o to 10o. However, the researchers achieved the topmost stability during the angle adjustments while continuing with their operations, so that they can be able to understand which the most suitable aerofoil model for them according to the velocity of wind that can vary from low or high, which will also be relevant with the conditions of weather in Iraq. From this study, it can be understood that the aerofoil model NACA 2418 is capable of having the most suitable angle of attack under any kind of circumstances that will be beneficial for both aircrafts and automobiles.

Rogowsk et al. [3] obtained values which are related to lift and drag coefficients for the Reynolds number of 2.9 million which also appropriately matches with the various predictions obtained from the experiments and from XFOIL over a diverse angle of attack ranges. Along with that, a maximum power coefficient router of around 0.5 is accumulated that results in making the impeller more attractive as the topic of further research purposes. These experiments also provide the future researchers with a better clarity regarding their choice of aerofoil for their study or experiment purposes. Sarucan and Sofuoğlu [4] experimented and observed that even minute changes within the models of the aircrafts and sports focused automobiles like the F1 cars have a major impact on their performance records. They experimented over various NACA aerofoil models as the primary design for rear wings of F1 cars, and they observed that by changing the crucial variables like the thickness, the angle of attack and the chord length of an aerofoil model or even fractional changes can have major impacts on the rear wing performance of an F1 car. Wang et al. [5] observed that for airfoil performance, maximum thickness and thickness positions leads to different ammounts of power. Young et al. [6] studied the distinct properties related to the formulation of ABF's during their experimentations, keeping in contrast with the method of fundamental solutions (MFS) by implementing the RBF's. The ABF's collection method was incorporated for dealing with discontinuous or uneven boundaries more accurately. During their study both the exterior as well as the interior problems related to the potential flow which are governed by the 2D Laplace equations are also explored with the help of RBF's and ABF's schemes for various comparison activities. They also tested a cusp cavity, a square cavity and a uniform flow within a circular cylinder along with the aerofoil model NACA-2418 for examining the demerits and merits off both the RBF's and ABF's formulations. Singh et al. [7] optimized the analysis of two-dimensional airfoils to determine the wind turbine blade design that would yield the required power output. When Tokul et al. [8] analyzed many characteristics, including power coefficients, pressure distribution on the blades, and coefficients of lift and drag, they discovered that, for small diameter wind turbines, the NACA 6409 airfoil was more efficient than the NACA 2414 airfoil. Loutun et al. [9] investigated the performances related to the aerodynamics of NACA airfoils. The geometrical shape and curves of an aerofoil design were created to maximize lift and reduce drag. The camber, angle of attack, and thickness distribution of the aerofoil design, all have various impacts upon the behaviour of the boundary layer were discussed in detail innthis study. Bramantya and Ginting [10] studied that thee output from their design study requires ideal CL and CD values for receiving the optimal performance of their aircraft design. Ranjbaran [11] concluded that the quality related with the results derived from simulation was majorly influenced by the size of the mesh as well as the grid size. Shih and Hsu [12] carried out an analysis regarding an enhanced k-ε model related to close wall turbulence.

2. Objectives

The authors found inadequate number of researches on performance optimization of NACA 2418 airfoil at higher Reynolds number. The objective of this article is to effectively understand the procedure to model flow over NACA 2418 airfoil numerically and to find optimimum operating condition for the same, typically at higher Renolds number (i.e. $Re = 5 \times 10^6$ and 7×10^6). Along with that, this paper also aims to focus on the study of the distribution of the flow parameters like pressure, velocity over the domain.

3. Methodology

The methodology part will be described in five segments: Governing equations and turbulence model, problem geometry, grid generation, boundary conditions and materials properties, and numerical simulation.

3.1 Governing equations and turbulence model

The basic equation of numerical modelling is Navier-Stoke's equation [13]. The first equation in this is the continuity equation which can be expressed as follows:

$$\frac{\partial \rho}{\partial t} + \nabla.\left(\rho \vec{V}\right) = 0 \tag{1}$$

The second equation i.e. Conservation of momentum may be expressed as:

$$\rho\left(\frac{\partial \vec{V}}{\partial t} + \left(\vec{V}.\nabla\right)\vec{V}\right) = -\nabla p + \mu\nabla^2\vec{V} + \rho\vec{g} \tag{2}$$

The above equations are considered with usual nomenclature for density, velocity, pressure, dynamic viscosity and gravitational acceleration designated by by ρ, $\vec{V}$, p, μ and $\vec{g}$, respectively.

The transport equations for turbulent kinetic energy (k) and turbulent dissipation rate (ε) are as given below.

$$\frac{\partial(\rho k)}{\partial t} + \frac{\partial(\rho k V_i)}{\partial x_i} = \frac{\partial}{\partial x_j}\left[\frac{\mu_t}{\sigma_k}.\frac{\partial k}{\partial x_j}\right] + 2\mu_t E_{ij}E_{ij} - \rho\epsilon \tag{3}$$

$$\frac{\partial(\rho \varepsilon)}{\partial t} + \frac{\partial(\rho \varepsilon V_i)}{\partial x_i} = \frac{\partial}{\partial x_j}\left[\frac{\mu_t}{\sigma_\varepsilon}.\frac{\partial \varepsilon}{\partial x_j}\right] + C_{1\varepsilon}\frac{\varepsilon}{k}2\mu_t E_{ij}E_{ij} - C_{2\varepsilon}\rho\frac{\varepsilon^2}{k} \tag{4}$$

where V_i denotes the velocity component in the corresponding direction, μ_t denotes the eddy viscosity and E_{ij} represents the component of the rate of deformation.

3.2 Problem Geometry

The aerofoil model NACA-2418 is a NACA four digit aerofoil having a maximum width of 18% at 30% chord along with a maximum chamber of 2% at 40% chord. The four-digit aerofoils are signified as NACA xxxx, within which the first digit signifies the maximum chamber as a percentage of the chord. The second digit signifies the distance of the maximum chamber with accordance to the aerofoil's leading edge in tenths of the model's chord and the last two digits signifies the maximum thickness of the model as a percentage with accordance to its chord. Figure 1 describes the problem geometry in detail. For the creation of the aerofoil geometry in the Space Claim, the aerofoil data is collected from the Airfoil Tools website (http://airfoiltools.com). After that, the data of the aerofoil model was selected and copied on to a new excel sheet where the data then is structured into a table format. Within the table the data of the aerofoil model is divided into three columns that represents its three planes x, y and z. Along with that, it is also clarified that the 3d value of the aerofoil design will be true and the polyline value of the aerofoil design will also be true. The excel sheet is to be saved in (.txt) format. Then within the Space Claim Geometry, changes such as the length unit is selected as Meters (m) and the primary precision is taken as 5.

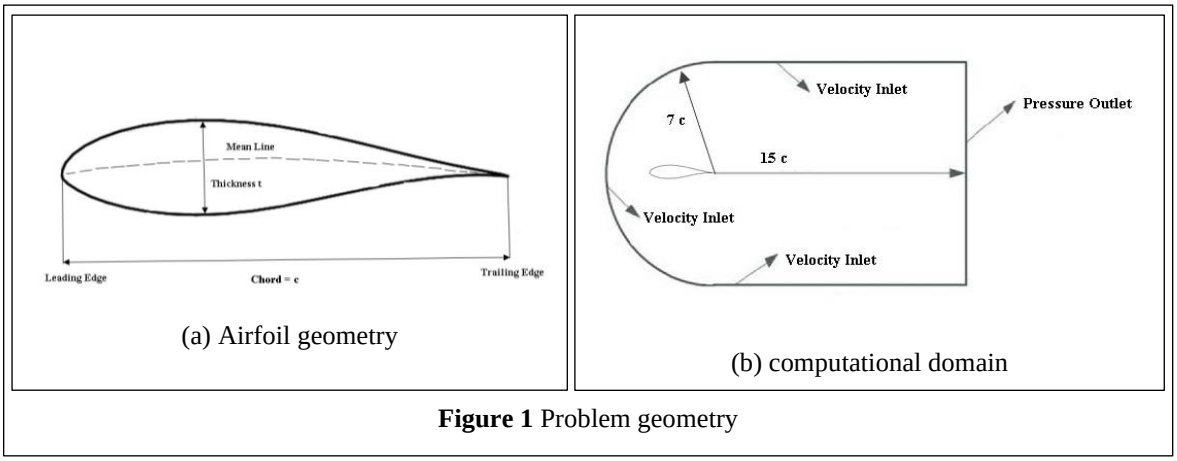

(a) Airfoil geometry

(b) computational domain

Figure 1 Problem geometry

3.3 Grid generation

A triangle dominant 2-D mesh system has been chosen to discretize the CFD-domain. Element sizes are set to 0.3 m and along with a hard behaviour scheme in the Ansys-mesh. Inflation is given with number of layers equal to 10 and a maximum thickness of 0.006 m. The entire mesh has 24199 numbers of nodes. The minimum orthogonal quality is 0.013. This optimum grid is chosen by a suitable grid-independence study. The grids are displayed in Figure 2.

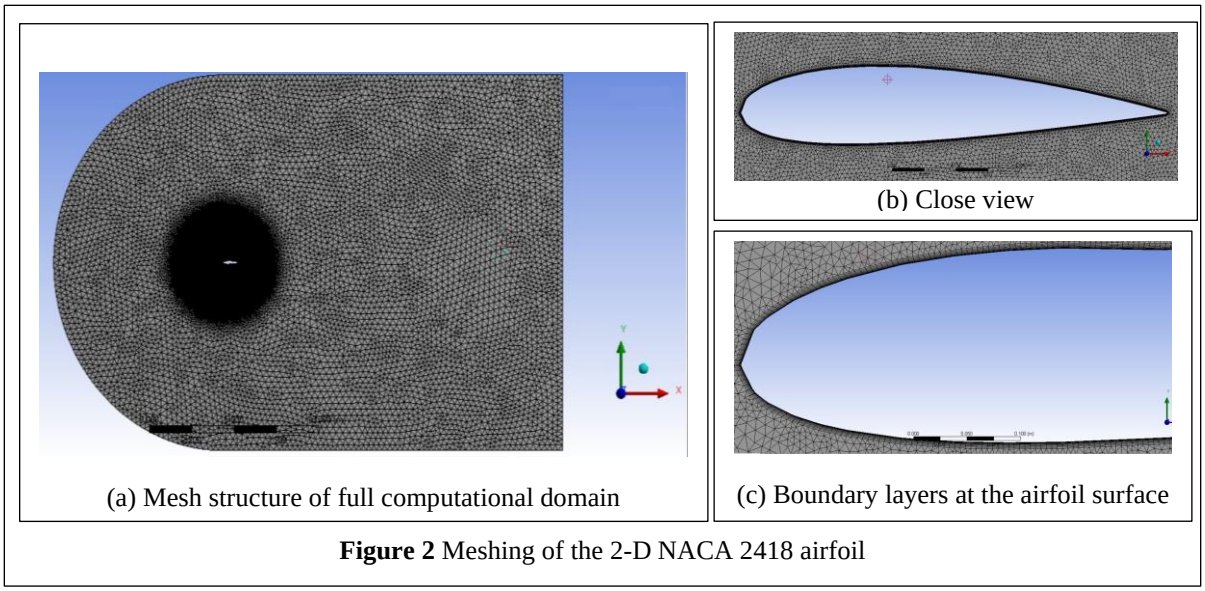

(a) Mesh structure of full computational domain

(b) Close view

(c) Boundary layers at the airfoil surface

Figure 2 Meshing of the 2-D NACA 2418 airfoil

3.4 Boundary conditions and materials properties

The airfoil surface has been set to stationary wall having no slip, no penetration boundary condition. The surface of the airfoil is considered as aluminium aloy made smooth surface. The inlet is set as velocity inlet (shown in Figure 1), where the velocity magnitude is determined by Re of the flow. Inlet velocities are chosen as 49.55 and 69.78 m/s for $Re = 5 \times 10^6$ and $Re = 7 \times 10^6$ respectively. The outlet pressure is set to the atmospheric pressure. The direction of the velocity is set by the x and y-component of velocity, which is to be determined from the angle of attack (α). The flowing fluid is chosen as air, having a density equal to 1.205 kg/m^3. Dynamic viscosity of the air is chosen as 1.821×10^5Ns/m^2. The temperature was set to 298 K.

3.5 Numerical Procedure

For the pressure-velocity coupling, the Semi-Implicit Method for Pressure-Linked Equations (SIMPLE) scheme was chosen, while the green-gauss node based approach was chosen for the spatial discretization part. To find the optimal solution, the turbulent kinetic energy, turbulent dissipation rate, and momentum were calculated using the second order upwind method. The turbulence model is chosen as the standard k-ε model with scalable wall function. The solution is initialized by hybrid mode. The convergence criteria is set as the residual value equal to 10^{-7}.

4. Results and Discussion

4.1 Validation

The lift coefficient is generally calcuted using the following equation:

$$F_L = C_L(\tfrac{1}{2}\rho V^2) \tag{5}$$

Where, F_L is the lift force, C_L is the lift coefficient.
Similarly drag coefficient can also be calculated using the following expression:

$$F_D = C_D(\frac{1}{2}\rho V^2) \quad (6)$$

Where, F_D is the drag force, C_D is the drag coefficient. The numerical results are validated against the experimental results [14], which have been shown in Figure 3. We can see the numerical results obtained from the present simulation ($Re = 5 \times 10^6$) are in good agreement with the experimental results. This indicates the suitability of the model.

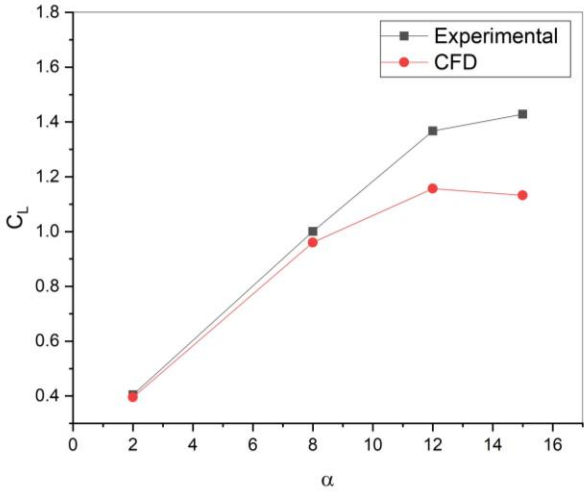

Figure 3 Comparison of numerically calculated C_L with experimental data

4.2 Variation of Lift and Drag coefficient

The lift and drag coefficients (C_L and C_D) are plotted against different α in two Reynolds number, $Re = 5 \times 10^6$ and $Re = 7 \times 10^6$ and shown in Figure 4. The plot reveals that both C_L and C_D are dependent on the value of α. We observe a gradual rise in the value of C_L followed by a gradual fall as the α value increases from 0 to 18 degree.

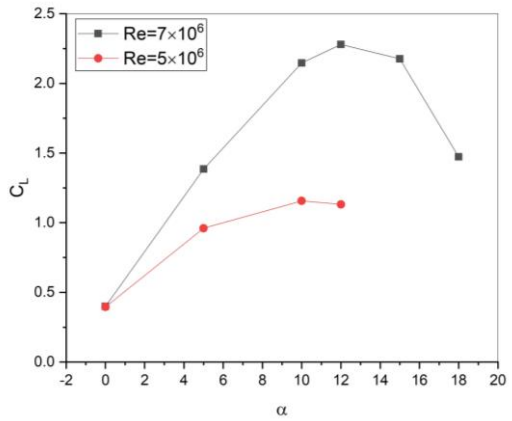

Figure 3 C_L for different α

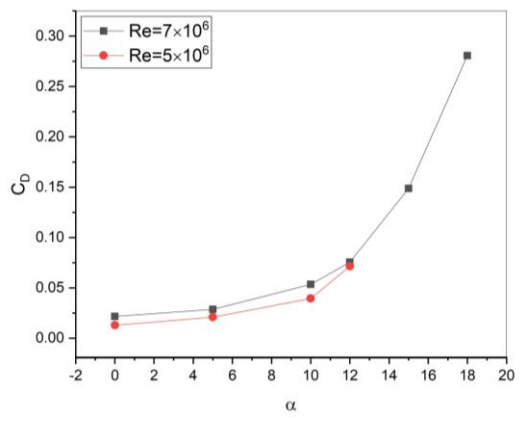

Figure 4 C_D for different α

The value of C_L for any α is found to be higher with the increase in Re. The maximum C_L for $Re = 5 \times 10^6$ found to be near $\alpha = 10^o$, whereas for $Re = 7 \times 10^6$ the maximum value for C_L is achieved near $\alpha = 12^o$.

These α values are called 'critical angle of attack' or 'stall angle of attack'. Maximum lift with minimum drag is always intended. Thus we plot variation of Lift to drag ratio in Figure 5.

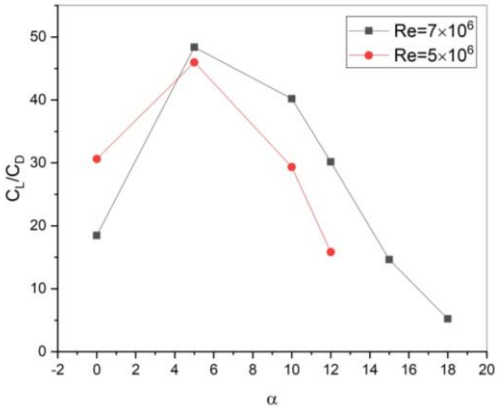

Figure 5 Variation of C_L/C_D with α

Lift to drag ratio is found to be first increasing then decreasing in rapid manner with the increase of α for both of the Re. We obtain a maximum C_L/C_D near about $\alpha = 5^o$ for both the Re.

4.3 Pressure & Velocity contours

In order to understand the performance of the airfoil in detail, we need to vizualize the pressure and velocity distribution over the entire domain. Thus we plot the pressure and velocity contours for α varying from 0 to 18 degree. Pressure and velocity contours at $\alpha = 15^o$ for two different Re are compared in Figure 6.

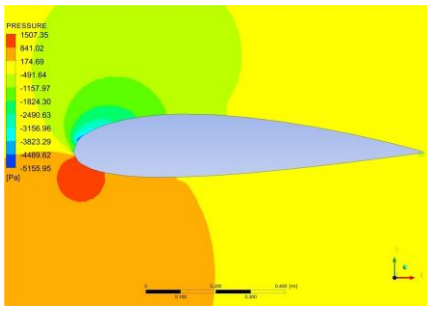

Figure 6 (a) Pressure contour at α =15º, $Re = 5 \times 10^6$

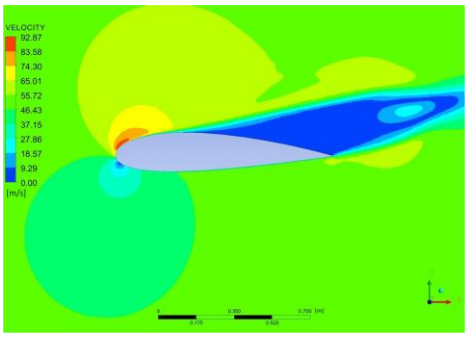

Figure 6 (b) Velocity contour at α =15º, $Re = 5 \times 10^6$

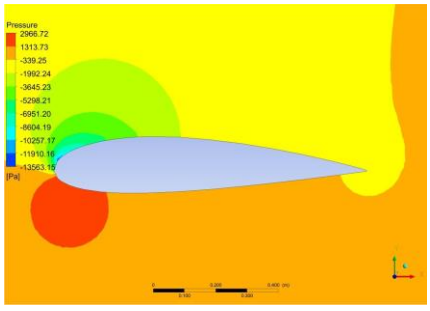

Figure 6 (c) Pressure contour at α =15º, $Re = 7 \times 10^6$

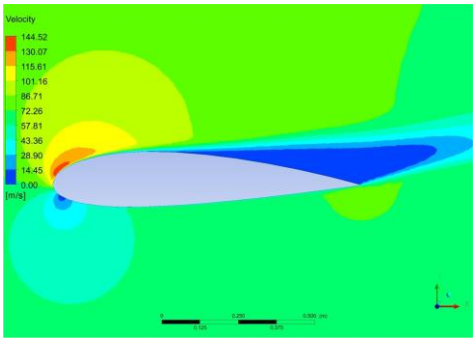

Figure 6 (d) Velocity contour at α =15º, $Re = 7 \times 10^6$

We may compare pressure contours at Figure 6(a) and 6(c) for $Re = 5 \times 10^6$ and $Re = 7 \times 10^6$ respectively. We observe higher pressure zone just at the bottom of leading edge, and lower pressure zone just at the top of the same edge for this α. This higher pressure and lower pressure zones are found to be increased quantitatively in the higher Re case. We may recall our elimentary aerodynamic concept, that this difference in pressure creates the upward unbalanced force i.e. lift. As this difference becomes quantitatively higher with increase of Re, it is obvious that the lift will increase. In figure 6(b) and 6(d), we may compare velocity contours for $Re = 5 \times 10^6$ and $Re = 7 \times 10^6$ respectively. As an increase in pressure is always associated with a decrease in velocity, we can find the higher velocity zone to be appeared near the top corner of the leading edge of the airfoil and a corresponding lower velocity zone at the bottom corner of the same edge. We can also find wake behind the airfoil body, indicated by a large blue coloured (lower velocity) zone. This is due to flow separation. This wake is higher for a higher Re, which increase in drag with the increase in Re.

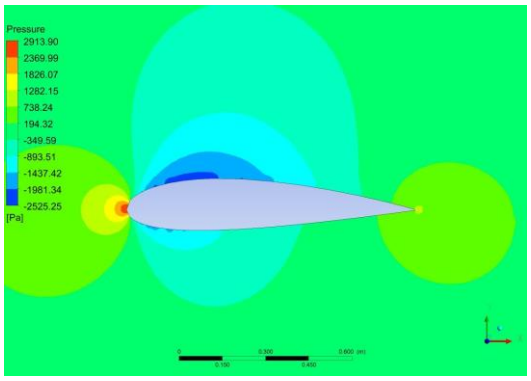

Figure 7(a) Pressure contour at α =0º, $Re = 7 \times 10^6$

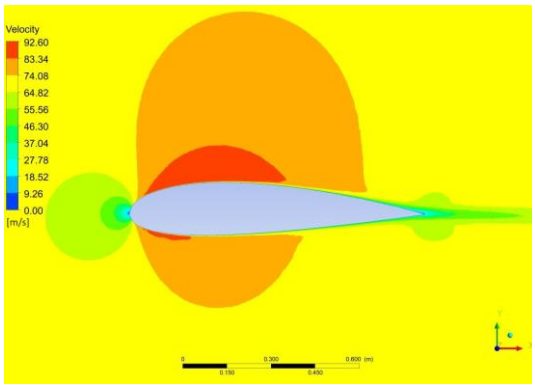

Figure 7(b) Velocity contour at α =0º, $Re = 7 \times 10^6$

We plot the pressure and velocity contours for a 0 degree angle of attack for $\mathrm{Re} = 7 \times 10^6$ in Figure 7(a) and 7(b). We observe the higher pressure (indicated by red colour) zone is exactly at the tip of the leading edge. The lower pressure zone is near the upper surface of the airfoil. The difference in the pressure at the upper and lower surface is not very high, that is why lift generation at this angle of attack is also moderate. Velocity contour depicts the higher velocity zone to be appearing exactly at the location of lower pressure zone and vice-versa. The flow-separation and wake formation is also in lesser amount at this angle of attack.

In Figure 8, pressure and velocity contours for α =5º, 12º and 18º has been plotted for $\mathrm{Re} = 7 \times 10^6$. It can be clearly observed that higher pressure zone (red coloured) as well the difference in pressure between upper and lower surface of the airfoil has been increased from α =5º to 12º, and then at α =15º, these has been decreased a little bit. This behaviour can be considered as am explanation of the rising followed by falling trend of C_L.In the velocity contours, we found the zone of flow separation (blue shaded) behind the airfoil changes its orientation increases and becomes stronger as the α increases from 5º to 12º and 12º to 18º. This is an explanation for the continuous increase in C_D with the increase of angle of attack.

6. Conclusion

From the above discussion on the numerical results related to flow over NACA 2418 airfoil at Reynolds numbers 5×10^6 and 7×10^6 we may conclude as following :

- The the standard k-ε turbulence model is utized suitably to model the present problem. The results are in a good agreement with the previous experimental result.
- Lift coefficient is found to be first increasing then decreasing as the angle of attack increases.

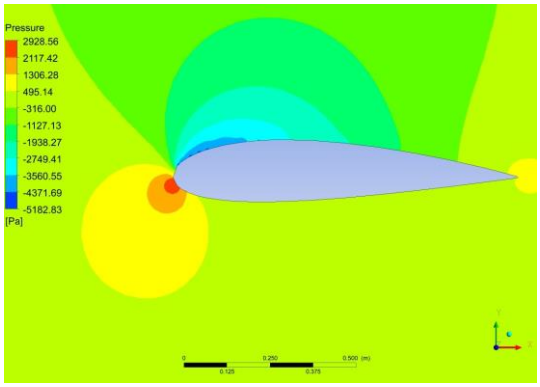

Figure 8(a) Pressure contour at α =5º, $Re = 7 \times 10^6$

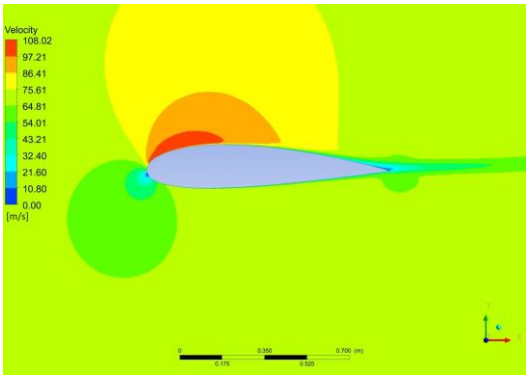

Figure 8(b) Velocity contour at α =5º, $Re = 7 \times 10^6$

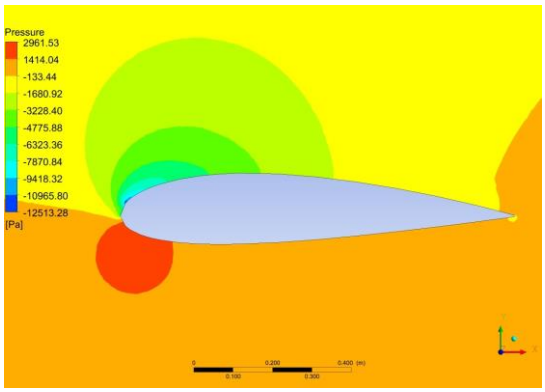

Figure 8(c) Pressure contour at α =12º, $Re = 7 \times 10^6$

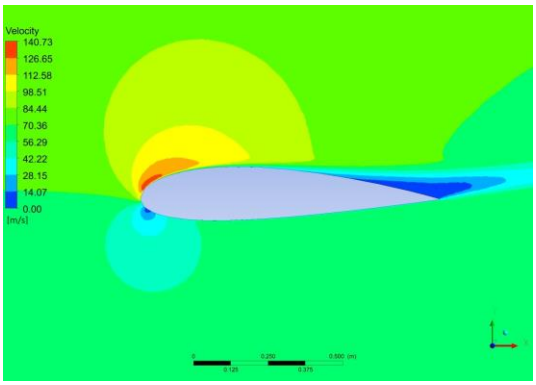

Figure 8(d) Velocity contour at α =12º, $Re = 7 \times 10^6$

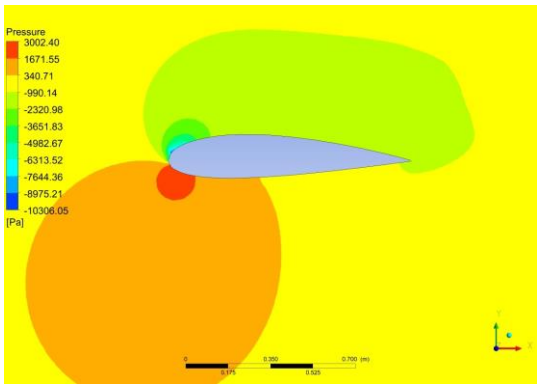

Figure 8(e) Pressure contour at α =18º, $Re = 7 \times 10^6$

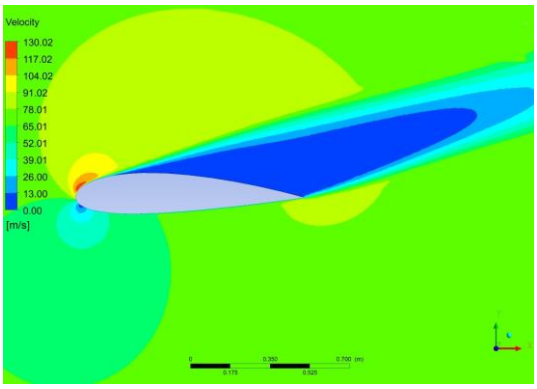

Figure 8(f) Pressure contour at α =18º, $Re = 7 \times 10^6$

- The stall angle of attack is found to be higher at higher Reynolds number (10º for 5×10^6 and 12º for 7×10^6).
- The drag coefficient is continuously increasing with the increase of angle of attack.
- The optimum lift to drag ratio is found at 5º for both the Re.
- The phenomenon of lift and drag can be suitably explained by the pressure and velocity contours.

Nomenclature

Angle of Attack	$\boldsymbol{\alpha}$
Lift coefficient	$\boldsymbol{C_L}$
Drag coefficient	$\boldsymbol{C_D}$
Turbulent kinetic energy	$\boldsymbol{k}$
Turbulent dissipation rate	$\boldsymbol{\varepsilon}$
Velocity	$\boldsymbol{V}$
Computational Fluid Dynamics	$\boldsymbol{CFD}$
Reynolds Number	$\boldsymbol{Re}$

Refrences

[1] Graham IV, H. Z., Panther, C., Hubbell, M., Wilhelm, J. P., Angle, G. M., & Smith, J. E. (2009, January). Airfoil selection for a straight bladed circulation controlled vertical axis wind turbine. *In Energy Sustainability*, Vol. 48890, pp. 579-584.

[2] Abood, Y. A., Abdulrazzaq, O. A., Habib, G. S., & Haseeb, Z. M. (2022). Determination of the Optimum Aerodynamic Parameters in the Design of Wind Turbine Using COMSOL Multiphysics Software. Iraqi *Journal of Industrial Research*, 9(2), 77-85.

[3] Rogowski, K., Hansen, M. O. L., & Bangga, G. (2020). Performance analysis of a H-Darrieus wind turbine for a series of 4-digit NACA airfoils. *Energies*, 13(12), 3196.

[4] Sarucan, F., & Sofuoğlu, M. A., (2023). Optimizing Formula 1 rear wings with NACA series airfoils for maximum performance. 9. *Uluslararası Mühendislik ve Teknoloji Yönetimi Kongresi*, Turkey.

[5] Wang, Y., Shen, S., Li, G., Huang, D., & Zheng, Z. (2018). Investigation on aerodynamic performance of vertical axis wind turbine with different series airfoil shapes. *Renewable energy*, 126, 801-818.

[6] Young, D. L., Huang, Y. J., Wu, C. S., Sladek, V., & Sladek, J. (2015). Angular basis functions formulation for 2D potential flows with non-smooth boundaries. *Engineering Analysis with Boundary Elements*, 61, 1-15.

[7] Singh, R. P., Kumar, P., Sangha, G. S., & Labana, Z. D. (2022). Numerical Analysis of an Optimized Wind Turbine Blade. *In AIAA SCITECH 2022 Forum* (p. 0217).

[8] Tokul, A., & Unal, K. U. R. T. (2023). Comparative performance analysis of NACA 2414 and NACA 6409 airfoils for horizontal axis small wind turbine. *International Journal of Energy Studies*, 8(4), 879-898.

[9] Loutun, M. J. T., Didane, D. H., Batcha, M. F. M., Abdullah, K., Ali, M. F. M., Mohammed, A. N., & Afolabi, L. O. (2021). 2D cfd simulation study on the performance of various naca airfoils. *CFD Letters*, 13(4), 38-50.

[10] Bramantya, M. A., & Ginting, R. R. R. (2020, July). Study of the effect of 4-digit NACA variation on airfoil performance using computation fluid dynamics. *In AIP Conference Proceedings* (Vol. 2248, No. 1). AIP Publishing.

[11] Ranjbaran, B. (2021). Airfoil selection for a small-scale vertical axis wind turbine: a numerical study (Doctoral dissertation).

[12] Shih, T. H., & Hsu, A. T. (1991). An improved k-epsilon model for near wall turbulence. NASA. Lewis Research Center, Center for Modeling of Turbulence and Transition (CMOTT). Research Briefs: 1990.

[13] White, F. M., & Majdalani, J. (2006). Viscous fluid flow (Vol. 3). New York: McGraw-Hill.

[14] Abbott, I. H., & Von Doenhoff, A. E. (2012). Theory of wing sections: including a summary of airfoil data. Courier Corporation.